Static and dynamic properties of annular Josephson junctions with injected current

D. Perez de Lara, M. P. Lisitskiy, C. Nappi, and R. Cristiano

C.N.R.-Istituto di Cibernetica "E. Caianiello," via Campi Flegrei 34, I-80078 Pozzuoli, Napoli, Italy

(Received 30 December 2005; revised manuscript received 6 April 2006; published 29 June 2006)

We have investigated theoretically and experimentally a *small* annular Josephson junction with three leads, where the third lead is added to one of the ring-shaped electrodes to apply a control (injection) current and thereby create a local magnetic field. We study the static case, namely, we derive the general expression for the Josephson critical current in the presence of both an injection current and an external parallel magnetic field. Concerning the theoretical investigation of the dynamic case, we obtain an analytical expression for the Fiske steps amplitude as a function of the injection current intensity and the angle separating the two injection leads (θ_1). The theoretical results show that a perfect analogy with the behavior of a rectangular junction in an external uniform magnetic field can be established for any orientation of the injector leads in the static case, while in the dynamic case the analogy holds only when the injector leads have a separation angle of $\theta_1 = \pi$. We present experimental dependences of the Josephson critical current and Fiske steps amplitudes on the injected current for two separation angles $\theta_1 = \pi/2$ and $\theta_1 = \pi$. The analysis and the comparison with the experiments confirm the theoretical predictions. The Fiske step measurements, presented for the case $\theta_1 = \pi/2$, have no straightforward analogous for the rectangular junction; however, we show a very good agreement between theory and experiments also in this case.

I. INTRODUCTION

An attractive property of annular Josephson tunnel junctions (AJTJs) is certainly represented by their ability to trap *permanently* quantized magnetic flux in the form of flux quanta or fluxons. Fluxons motion is particularly simple in these structures because of the absence of fluxon-open boundary collisions. For these reasons, AJTJs have been usefully employed to establish much of the present knowledge about fluxon dynamics.[1–3] At present, AJTJs are also under investigation for their connection with several fundamental issues and applications, such as laboratory testing of cosmological scenarios,[4] quantum computation,[5] and radiation detection.[6,7] In all these contexts, the fluxon trapping phenomenon, either induced or spontaneous, is a basic process to be fully understood and possibly controlled. Both *small* and *long* annular junctions, i.e., junctions with the external diameter smaller or larger than the Josephson penetration length, λ_j,[8] have been investigated. Trapping of fluxons in *long* AJTJs has been demonstrated many times and is currently being used. Flux trapping in *small* junctions is conceptually and practically more difficult, although it has been realized in experiments.[6–9] However, a complete control of the trapping process remains an issue to be addressed, mostly if one wants to rely on a simple methodology.

An interesting configuration of AJTJs was proposed in Ref. 10. In that configuration, an additional lead is added to one electrode (the control electrode), as shown in Fig. 1. In this way, a circulating current can be injected in the control electrode to generate a magnetic field through the tunneling barrier. The counterelectrode has one lead only, which collects the tunneling current. The current injection represents a promising method to simulate (and study) the flux quanta trapping inside the ring electrodes of annular junctions. It also represents an interesting alternative possibility for the use of external coils to generate the magnetic field in order to suppress the Josephson critical current, which remains a major relevant issue in the framework of radiation detectors based on superconducting tunnel junctions (STJs).[6,7]

Stimulated by preliminary experimental results presented in Ref. 10, in a previous paper[11] we developed the basic analytical theory of dc electromagnetic properties of a *small* AJTJ with a current injected in the control electrode. The theoretical analysis presented in Ref. 11 showed that the Josephson critical current, I_c, modulates with the magnetic field generated by the injection current, I_{inj}, according to the Fraunhofer diffraction pattern. It is well known that the Fraunhofer pattern is the usual result observed in connection with *small* rectangular Josephson junctions in the presence of an external uniform magnetic field.[12] More recently, it has been theoretically shown that the Fraunhofer behavior holds also for the case of current injection in arbitrarily *long* AJTJs.[13] Notably, the analysis performed in Ref. 11 also demonstrated that injected currents can produce magnetic field configurations very similar to, and in many aspects, undistinguishable from the effect of the presence of truly trapped flux quanta.

In this paper, we report on further developments regarding the investigation of an AJTJ with injected current. We derive the general theoretical expression for the Josephson critical current in the presence of both an injection current and an external parallel magnetic field. We carry out the theoretical analysis of ac properties (Fiske resonances) of an AJTJ when the injection current is applied. We present experimental data which will be compared with the theoretical predictions of our model both for the dc and ac case. In this work, we still remain in the framework of *small* annular junctions. This ensures that the screening effect of the tunneling current can be neglected, so that the analysis is greatly simplified and the comparison with the experiments appears clear and precise. In particular, our experiments confirm the theoretical prediction of Fraunhofer modulation of the $I_c(I_{inj})$ pattern and that the period of the I_c modulation is determined by the angle θ_1
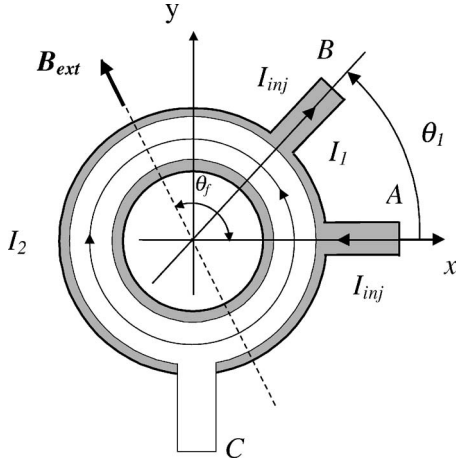
FIG. 1. Schematic of an annular Josephson junction with injection current leads. The injection current I_{inj} is applied through leads A and B into the bottom electrode. A bias tunneling current I_b, flowing from one electrode (leads either A or B) to the other (C) is used to measure electrophysical properties of the tunnel junction barrier. $\mathbf{B}_{ext}$ is the external magnetic field applied parallel to the barrier plane.

between the injector leads in the control electrode, and by the self-inductance value of the ring-shaped control electrode. The experiments are made for two different values of the separation angle $\theta_1 = \pi$, $\pi/2$. This demonstrates the general validity of our theoretical model. Measurements of I_c on the external magnetic field, in the presence of injected current, confirm as well the prediction of Ref. 11 and clearly show the similarity of the phenomenology with the truly trapped case. We also investigate the dynamics (ac properties, Fiske resonances) of the AJTJ with injection current within the framework of the Kulik theory of Fiske steps.[14] Injection of a current in one of the ring electrodes generates a magnetic field in the plane of the annular barrier and, as is well known, under this condition resonances known as Fiske steps appear in the current-voltage characteristic of the junction. These resonances are a consequence of the interaction of the ac Josephson effect and the normal modes of the electromagnetic cavity of the junction. We present experimental results that show how the variation of the separation angle θ_1 between the leads, which governs the uniformity of the radial magnetic field in the barrier plane, introduces significant changes in the dynamical states represented by the Fiske resonances, which are in good agreement with our theory. We report the dependences of the first three Fiske step amplitudes on the injected current, obtained at two different separation angles between the injector leads $\theta_1 = \pi$ and $\pi/2$. Only in the symmetric case of $\theta_1 = \pi$, the radial magnetic field generated by the injected current has a uniform intensity. The second configuration here considered ($\theta_1 = \pi/2$), corresponds to the excitation of Fiske resonances in a Josephson junction by means of a nonuniform magnetic field.

The plan of the paper is as follows. Section II is dedicated to the theoretical investigation of the Josephson critical current and Fiske resonances of *small* annular junctions with an injected current and external parallel magnetic field. In Sec. III, a description of the sample details and the experimental

setup is reported. Next, in Sec. IV, we present the results of the experiments and the comparison with the theory. Section V states the derived conclusions.

II. THEORY

We consider the annular Josephson tunnel junction between two superconducting films schematically shown in Fig. 1. The injection current I_{inj} flows between leads A and B connected to the bottom electrode (the control electrode), with a separation angle θ_1. A third lead, C, on the top electrode (the counterelectrode), serves to feed the bias tunneling current I_b through the junction barrier when used together with one of the two bottom leads, A or B. An external magnetic field, $\mathbf{B}_{ext}$, oriented parallel to the junction barrier, is also considered. We note that this junction configuration slightly differs from the one previously presented in Ref. 11. In fact, in experiments presented in this paper, the configuration illustrated in Fig. 1 is used with the bottom electrode containing the junction leads.

A. General relation for the phase difference

We begin by giving the general expression for the phase difference in the presence of both an external magnetic field and an injected current. The external uniform magnetic field $\mathbf{B}_{ext}$ can be written in terms of the radial and azimuthal components in polar coordinates as

$$\mathbf{B}_{ext} = B_{ext,r}\hat{\mathbf{r}} + B_{ext,\theta}\hat{\boldsymbol{\theta}} = B_{ext}\cos(\theta_f - \theta)\hat{\mathbf{r}} + B_{ext}\sin(\theta_f - \theta)\hat{\boldsymbol{\theta}},$$
(1)

where θ_f is the angle between $\mathbf{B}_{ext}$ and the x axis. We approximate the injection current distribution inside the control electrode assuming that the currents have only θ components. Therefore, the magnetic field generated by the injected current has only a radial component and, in the case of a small width of the control annular electrode, can be written as

$$\mathbf{B}_{inj} = \begin{cases} -\dfrac{\phi}{\theta_1 r d_{eff}}\hat{\mathbf{r}} & 0 < \theta < \theta_1 \\[3mm] \dfrac{\phi}{(2\pi - \theta_1)r d_{eff}}\hat{\mathbf{r}} & \theta_1 < \theta < 2\pi, \end{cases}$$
(2)

where d_{eff} is the effective magnetic penetration depth, i.e., the sum of the barrier thickness and London penetration depths of the electrodes, ϕ is the magnetic flux generated by the injected current in each two sectors of the junction, determined by θ_1 and $2\pi-\theta_1$, respectively. In terms of the injection current I_{inj}, it writes $\phi = I_{inj}L^*$, where L^* is the parallel of the inductances of the two sectors (see Fig. 1). L^* is given by

$$L^* = L\theta_1(2\pi - \theta_1)/(2\pi)^2,$$
(3)

where L is the self-inductance of the control electrode, i.e., of the bottom annular electrode connected to the injection leads, and through which the current is actually injected, as was provided by the real sample configuration used in our
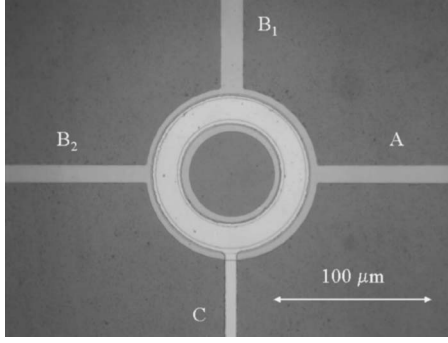
FIG. 2. Photograph of the Nb-based annular junction with three injection leads A, B_1, and B_2 on the bottom electrode and with the bias lead C on the top electrode.

experiment (see Figs. 1 and 2). Since the bottom electrode is covered by the superconducting top electrode, which acts as a superconducting ground plane, the value of L may differ greatly from that of an isolated plane ring. As a reasonable approximation, the self-inductance of the base annular electrode can be calculated by the formula for a thin-film loop deposited onto an infinite insulated ground plane[15]

$$L = \frac{2\pi\bar{r}\mu_0 d_{eff}}{wF}g, \qquad (4)$$

where F is the fringe factor, μ_0 is the permeability of free space, $w = R_2 - R_1$ is the width of the ring (R_1 and R_2 are the internal and external radius, respectively), and $\bar{r}$ is the mean radius of the ring $\bar{r} = (R_1 + R_2)/2$. We have introduced the factor g in order to take into account the deviation of the finite geometry of the top electrode with respect to the infinite ground plane approximation.

If any other magnetic field is neglected, the phase difference between the electrodes can be calculated through

$$\nabla\varphi = \bar{k}(\mathbf{B_{ext}} + \mathbf{B_{inj}}) \times \hat{\mathbf{z}}. \qquad (5)$$

Here, $\bar{k} = 2\pi d_{eff}/\Phi_0$ and $\Phi_0 = h/2e$ is the elementary magnetic flux quantum. Equivalently, Eq. (5) may be written as

$$\frac{\partial\varphi}{\partial r} = \bar{k}B_{ext,\theta},$$

$$\frac{\partial\varphi}{\partial\theta} = -\bar{k}r(B_{ext,r} + B_{inj}), \qquad (6)$$

whose solution is

$$\varphi = \kappa r\sin(\theta_f - \theta) + l(\theta) + \varphi_0. \qquad (7)$$

Here, $\kappa = \bar{k}(B_{ext,\theta}^2 + B_{ext,r}^2)^{1/2}$, φ_0 is a constant phase, and $l(\theta)$ is defined as

$$l(\theta) = \begin{cases} a\theta, & 0 < \theta < \theta_1 \\ b\theta + c, & \theta_1 < \theta < 2\pi, \end{cases}$$

$$a = \frac{2\pi}{\theta_1}\frac{\phi}{\Phi_0},$$

$$b = -\frac{2\pi}{(2\pi - \theta_1)}\frac{\phi}{\Phi_0},$$

$$c = \frac{(2\pi)^2}{(2\pi - \theta)_1}\frac{\phi}{\Phi_0}. \qquad (8)$$

It is useful to note that the phase difference φ in Eq. (5) may be written in terms of the fluxes of the magnetic fields $\Phi = \Phi_{ext} + \Phi_{inj}$ as

$$\varphi = 2\pi\frac{\Phi}{\Phi_0} + \varphi_0. \qquad (9)$$

Here, we have introduced the flux $\Phi_{ext} \equiv d_{eff}rB_{ext,\theta}$ due to the external field, and the flux due to the magnetic field originated by the injected current

$$\Phi_{inj} = \begin{cases} \phi\dfrac{\theta}{\theta_1} & 0 < \theta < \theta_1 \\ \phi\dfrac{\theta}{\theta_1 - 2\pi} & \theta_1 < \theta < 2\pi. \end{cases} \qquad (10)$$

B. Josephson critical current in the presence of both an injection current and an external magnetic field

It is well known that the Josephson current density may be written as

$$j = j_1\sin\left(2\pi\frac{\Phi}{\Phi_0} + \varphi_0\right) \equiv j_1\sin[\delta\varphi(\theta) + \varphi_0], \qquad (11)$$

where j_1 is the Josephson critical current density at zero-magnetic field. Integrating Eq. (11) over the junction area $S = \pi(R_2^2 - R_1^2)$, yields the Josephson current I as a function of Φ:

$$I(\Phi)/I_{c0} = \langle\cos\delta\varphi(\theta)\rangle\sin\varphi_0 + \langle\sin\delta\varphi(\theta)\rangle\cos\varphi_0, \qquad (12)$$

where $I_{c0} = j_1 S$ is the Josephson critical current in zero-injection current and zero-external magnetic field, and the brackets $\langle\ \rangle$ denote spatial averaging over the junction area. By maximizing Eq. (12) with respect to φ_0, the critical current I_c is calculated as

$$I_c/I_{c0} = \sqrt{\langle\sin\delta\varphi(\theta)\rangle^2 + \langle\cos\delta\varphi(\theta)\rangle^2},$$

$$\langle\sin\delta\varphi(\theta)\rangle = \frac{1}{S}\int_{R_1}^{R_2}rdr\int_0^{2\pi}d\theta\sin[\kappa r\sin(\theta_f - \theta) + l(\theta)],$$

$$\langle\cos\delta\varphi(\theta)\rangle = \frac{1}{S}\int_{R_1}^{R_2}rdr\int_0^{2\pi}d\theta\cos[\kappa r\sin(\theta_f - \theta) + l(\theta)].$$

$$(13)$$

C. Calculation of Fiske resonances excited by injection current

In this section, we calculate the self-resonances of the AJTJ in the presence of the injected current and $\mathbf{B_{ext}} = 0$. This

calculation is based on the Kulik theory of Fiske steps.[14,16] We eliminate, for simplicity, any dependence on the r coordinate. In other words, we treat the one-dimensional (1D) problem by fixing r to the mean radius of the junction, $\bar{r} = (R_1+R_2)/2$. So, we expect that this theory does not apply to the case of a small inner radius junction when the geometry tends to a disk rather than a ring.

An important point to be noted here is the following. The equation governing the quantum mechanical phase difference in a 1D annular junction, in the presence of an external magnetic field, was established by Gronbech-Jensen *et al.*[2] This, apart from a further damping term which is unessential here, writes

$$\frac{\partial^2 \varphi}{\partial x^2} - \frac{\partial^2 \varphi}{\partial t^2} - \sin \varphi = \Delta \frac{\partial}{\partial x}(\mathbf{B} \cdot \mathbf{n}) + \alpha \frac{\partial \varphi}{\partial t} - \gamma, \quad (14)$$

where **B** is the normalized magnetic field, **n** is a unit vector in the direction of the normalized self-induced flux density within the junction, $\partial \varphi / \partial x$. α and γ are the damping and current driving terms, respectively, Δ is the coupling between the external field and the junction.

The 1D approximation together with the curvature associated with the annular geometry implies that the new term, $\Delta \partial / \partial x (\mathbf{B} \cdot \mathbf{n})$, appears. This term is absent in the usual equation describing a long 1D linear junction. As far as $\boldsymbol{B}_{ext}=0$, the magnetic field we consider here has only radial components [see Eq. (2)], so that $\mathbf{B} \cdot \mathbf{n}$ is a constant and $\Delta \partial / \partial x (\mathbf{B} \cdot \mathbf{n})$ is zero in our case as for the linear junction case (in the notation of the present paper, **n** coincides with $\hat{\mathbf{r}}$). We also assume that the quality factor Q of the junction electromagnetic cavity is low.[14] Then, we start by seeking solutions of the equation for the self-induced perturbation voltage v. The total tunnel barrier voltage, $V=(\Phi_0/2\pi)\partial\varphi/\partial t$, will be written as $V=V_0+v$, where V_0 is the dc part of the total voltage corresponding to the Josephson frequency $\omega=2\pi V_0/\Phi_0$. Then, the problem reduces to finding the solution of the equation:[16]

$$\frac{\partial^2 v}{\partial \theta^2} - \frac{\bar{r}^2}{\bar{c}^2}\frac{\partial^2 v}{\partial t^2} - \frac{\omega}{Q}\frac{\bar{r}^2}{\bar{c}^2}\frac{\partial v}{\partial t} = \frac{\Phi_0}{2\pi}\frac{\omega \bar{r}^2}{\lambda_j^2}\frac{\partial j}{\partial t}, \quad (15)$$

with the condition that $v(\theta,t)$ is a 2π periodical function of θ; $\bar{c}=(d/\mu_0\varepsilon d_{\text{eff}})^{1/2}$ is the Swihart velocity, ε is the relative dielectric permeability of the oxide barrier, $\lambda_j=(\Phi_0/2\pi\mu_0 j_1 d_{\text{eff}})^{1/2}$ is the Josephson penetration depth. The technique to solve Eq. (15) consists of replacing the current term by its lowest-order approximation $j \approx \sin[\omega t - l(\theta)]$, where $\varphi_0=\omega t - l(\theta)$ is the unperturbed phase, resulting in

$$\frac{\partial^2 v}{\partial \theta^2} - \frac{\bar{r}^2}{\bar{c}^2}\frac{\partial^2 v}{\partial t^2} - \frac{\omega}{Q}\frac{\bar{r}^2}{\bar{c}^2}\frac{\partial v}{\partial t} = \frac{\Phi_0}{2\pi}\frac{\omega \bar{r}^2}{\lambda_j^2}\cos[\omega t - l(\theta)], \quad (16)$$

where $l(\theta)$ is expressed by Eq. (8).

We seek solutions to Eq. (16) in the form

$$v = \sum_{k=0}^{\infty} \{[A_k^{(1)}\cos(k\theta) + A_k^{(2)}\sin(k\theta)]\cos(\omega t) + [B_k^{(1)}\cos(k\theta) + B_k^{(2)}\sin(k\theta)]\sin(\omega t)\}. \quad (17)$$

If Eq. (17) is substituted into the differential Eq. (16) and making use of the periodical boundary conditions, it is possible to show that the expansion coefficients have the forms:

$$A_k^{(1)} = \left(\frac{2\Phi_0\omega_j^2}{\omega}\right)\left(\frac{(1-k^2/\eta^2)R_k + T_k/Q}{(1-k^2/\eta^2)^2 + 1/Q^2}\right); \quad A_k^{(2)} = \left(\frac{2\Phi_0\omega_j^2}{\omega}\right)$$
$$\times\left(\frac{(1-k^2/\eta^2)S_k + U_k/Q}{(1-k^2/\eta^2)^2 + 1/Q^2}\right),$$

$$B_k^{(1)} = \left(\frac{2\Phi_0\omega_j^2}{\omega}\right)\left(\frac{(1-k^2/\eta^2)T_k - R_k/Q}{(1-k^2/\eta^2)^2 + 1/Q^2}\right); \quad B_k^{(2)} = \left(\frac{2\Phi_0\omega_j^2}{\omega}\right)$$
$$\times\left(\frac{(1-k^2/\eta^2)U_k - S_k/Q}{(1-k^2/\eta^2)^2 + 1/Q^2}\right), \quad (18)$$

where $\omega_j=\bar{c}/\lambda_j$, $\eta=\omega^2\bar{r}/\bar{c}^2$, and R_k, S_k, T_k, and U_k are given by the integrals

$$R_k(\phi) = \frac{1}{2\pi}\int_0^{2\pi} \cos l(\theta)\cos k\theta d\theta, \quad T_k(\phi)$$
$$= \frac{1}{2\pi}\int_0^{2\pi} \sin l(\theta)\cos k\theta d\theta$$

$$S_k(\phi) = \frac{1}{2\pi}\int_0^{2\pi} \cos l(\theta)\sin k\theta d\theta, \quad U_k(\phi)$$
$$= \frac{1}{2\pi}\int_0^{2\pi} \sin l(\theta)\sin k\theta d\theta, \quad (19)$$

where ϕ is the magnetic flux generated by the injection current (see subsec. II A of the present section), $k=1,2,3\ldots$.

Once the expansion for v is determined, the position and time-dependent phase may be written as[12]

$$\varphi = \omega t - l(\theta) + \frac{2\pi}{\Phi_0}\int_0^t v(t')dt' \equiv \omega t - l(\theta) + \varphi_1. \quad (20)$$

The net Josephson current density is given by $j=j_1\sin\varphi$. This current density is frequency modulated and contains a nonzero-dc term, which can be obtained by averaging on time

$$\langle j \rangle = \langle j_1\varphi_1 \cos \varphi_0 \rangle. \quad (21)$$

(now $\langle \ \rangle$ denotes the average on time. The time-independent spatially averaged critical current density J_{dc} is

$$J_{\text{dc}} = \frac{1}{2\pi}\int_0^{2\pi} \langle j \rangle d\theta. \quad (22)$$

It can be shown that J_{dc} is

$$\frac{J_{\text{dc}}}{j_1} = 2\pi \frac{\omega_j^2}{\omega^2} \sum_{k=1}^{\infty} \frac{(R_k^2 + S_k^2 + T_k^2 + U_k^2)/Q_k}{[1 - k^2\bar{c}^2/\omega^2\bar{r}^2]^2 + 1/Q_k^2}, \qquad (23)$$

where Q_k is the quality factor of the kth resonance. $Q_k \sim CR_d^k$, where C is the junction capacitance per unit length, and R_d^k is the voltage-dependent nonlinear tunneling resistance at the voltage position corresponding to the kth resonance. We note that the quality factor, Q_k, is also voltage dependent through R_d^k. It can be seen from Eq. (23) that whenever the condition $\omega\mathbf{r} = k\bar{c}$ is satisfied, a dc current peak is obtained at the voltage position

$$V_k = k\frac{\bar{c}}{\bar{r}}\frac{\Phi_0}{2\pi}; \quad k = 1, 2, 3 \dots . \qquad (24)$$

The magnitude of the dc current depends on the injected current whereas the magnitude of the kth peak is given by

$$\frac{J_k^F}{j_1} = 2\pi \frac{\bar{r}^2}{\lambda_j^2} \frac{Q_k}{k^2}(R_k^2 + S_k^2 + T_k^2 + U_k^2). \qquad (25)$$

In the case of $\theta_1 = \pi$ from Eq. (25), it is seen that the maximum amplitude of the kth Fiske resonance, as a function of the injection current, is given by

$$\frac{I_k^F}{I_{c0}} = \frac{\pi}{2} \frac{\bar{r}^2}{\lambda_j^2} \frac{Q_k}{k^2} F_k^2(\phi), \qquad (26)$$

where the function $F_k(\phi)^2$ is the same reported in Ref. 12 (p. 245). This means that the $I_k^F(\phi)$ dependence describing the kth Fiske resonance in the case of injected current at $\theta_1 = \pi$ is the same as that for a rectangular junction in the presence of uniform parallel magnetic field. This equivalence arises even if the field configuration in both cases is quite different. In the case of the injected current investigated herein, the magnetic flux changes sign twice, showing opposite signs in the two sections set by the leads at angle θ_1, whereas the sign of the flux in the case of a rectangular junction in an external parallel magnetic field remains unchanged along its side perpendicular to the magnetic field.

We stress however that the $I_k^F(\phi)$ theoretical dependence for the general case of $\theta_1 \neq \pi$ is not described by Eq. (26). Therefore the analogy of the Fiske step behavior of a "small" rectangular junction with that of an annular one is limited to the condition $\theta_1 = \pi$. All of these considerations are verified by the experiments presented in the next section.

III. EXPERIMENTS

We designed and fabricated a Nb-based annular junction with three injection leads at the bottom electrode and one at the top electrode. The photograph of the sample is shown in Fig. 2. This configuration allows one to make experiments with two separation angles between injection leads of $\theta_1 = \pi/2$ and $\theta_1 = \pi$. The external and internal diameters of the tunnel junction were $99 \pm 1 \ \mu$m and $61 \pm 1 \ \mu$m, respectively. The $\text{Nb}_{\text{bottom}}(150 \text{ nm})/\text{Al}(20 \text{ nm})/\text{Al}_2\text{O}_3/\text{Al}(20 \text{ nm})/\text{Nb}_{\text{top}}(50 \text{ nm})$ layers were deposited by dc magnetron sputtering in an Ar atmosphere onto a sapphire substrate. The aluminium oxide barrier, Al_2O_3, was grown by exposing the

surface of the Al layer deposited on the Nb base electrode to a static atmosphere of pure oxygen. The sample layers were patterned by photolithographic techniques. The proper configuration of the bottom electrode and the annular junction area were defined by reactive ion etching (RIE) of Nb layers in a CF_4/O_2 plasma and by wet etching of $\text{Al}/\text{Al}_2\text{O}_3/\text{Al}$ layers. A SiO film was then deposited as an insulating layer. The sample fabrication was completed by deposition of a Nb wiring of 400 nm and its patterning by the "lift-off" process.

The bias current was applied through leads C and A (see Fig. 2) in order to measure both the Josephson critical current and the amplitude of the Fiske resonances. The injection current was applied either through leads A and B_1 to obtain a separation angle of $\theta_1 = \pi/2$, or through leads A and B_2 corresponding to a separation angle of $\theta_1 = \pi$. In the experiments presented here, we also applied an external magnetic field, B_{ext}. A Helmholtz copper coil was used to generate this field. We considered only two possible orientations of B_{ext}: $\theta_f = \pi$ and $\theta_f = \pi/2$.

The measurements were carried out at $T = 4.2$ K in a shielded cryostat in order to prevent the influence of external electromagnetic noise. The Josephson critical current I_c was determined by measuring the switching current at $V = 10 \ \mu$V. The maximum amplitude of the Fiske resonances was determined by measuring the switching current of the resonance branch, and then subtracting the quasiparticle current at the voltage position of the Fiske resonaces.

We evaluated the junction parameters, d_{eff}, j_c, and λ_j, from the measurements of the $I_c(B_{ext})$ dependence with $I_{\text{inj}} = 0$. The effective penetration depth was $d_{\text{eff}} = 169$ nm. The Josephson critical current at $B_{ext} = 0$ was $I_c = 480 \ \mu$A, which gave a Josephson critical current density of $j_1 \sim 10 \text{A/cm}^2$. From these values, we can estimate the value of Josephson penetration depth $\lambda_j = 124 \ \mu$m, which ensures that we are in the *small* junction limit $R_2/\lambda_J < 1$.

IV. RESULTS AND DISCUSSION

A. Josephson critical current measurements

In this subsection, we present the results concerning the static behavior of an AJTJ with injected current. First, we will show the injected current modulation of the Josephson critical current in the absence of an external magnetic field. Then, we will show $I_c(B_{ext})$ patterns when fixed values of I_{inj} are circulating through the control electrode.

1. $I_c(I_{\text{inj}})$ dependence at $B_{ext} = 0$

Figure 3 shows the $I_c(I_{\text{inj}})$ dependences for separation angles $\theta_1 = \pi/2$ and $\theta_1 = \pi$, in absence of external magnetic field ($B_{ext} = 0$). Open circles are the experimental data, the solid lines are the theoretical curves that were calculated by using Eq. (6) from Ref. 11:

$$I_c(I_{\text{inj}}) = I_{c0} \left| \frac{\sin \pi(I_{\text{inj}}L^*/\Phi_0)}{\pi(I_{\text{inj}}L^*/\Phi_0)} \right|, \qquad (27)$$

where L^* was estimated by Eqs. (3) and (4). The geometrical factor g in Eq. (4) was the fit parameter. In accordance with the dependence of the fringe factor F on the ratio w/s,[15] w/s
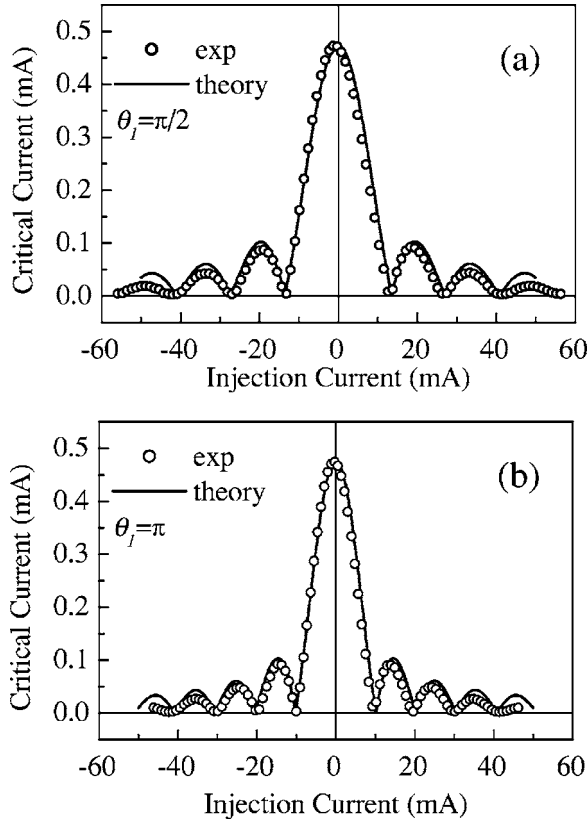
FIG. 3. Experimental dependence (open circles) of the Josephson critical current on the injection current measured at a separation angle between the injection leads of $\theta_1 = \pi/2$ (a) and $\theta_1 = \pi$ (b). The solid lines are the theoretical Fraunhofer-type curves calculated from Eq. (27).

FIG. 4. Sketch of the magnetic field line distribution created by an injection current in an annular Josephson tunnel junction. (a) Separation angle $\theta_1 = \pi$. The magnetic field in the tunnel barrier is radially and uniformly distributed in both sectors. The two fields are equal in magnitude and opposite in direction. (b) Separation angle of $\theta_1 = \pi/2$. The magnetic field in the tunnel barrier is radially distributed in both sectors, but the magnetic field intensity in the large sector 2 is less than in the small sector 1. The two fields are opposite in direction. For both separation angles the two magnetic fluxes have the same value of $\phi_1 = \phi_2 = L^* I_{\text{inj}}$. The dashed line represents the trajectory of the Josephson current wave exciting the Fiske resonances.

is a very large number in our case so that we can consider $F=1$ (s is the distance between the ground plane and the annular shape film, which is about the thickness of the tunnel barrier, i.e., few nanometers). Experimental data exhibit a clear Fraunhofer dependence for both values of the separation angles θ_1. The best agreement between theory and experimental data was obtained for $g=0.41$. This value is the same in all theoretical calculations used in this section. With this value, we estimated that the self-inductance L of the base electrode is of $L=8.1 \times 10^{-13}$ H instead of the value $L=2.0 \times 10^{-13}$ H as calculated for an infinite extension ground plane. Hence, the superconducting top electrode more effectively lowers the self-inductance of the base electrode in comparison with the infinite superconducting ground plane.

From Figs. 3(a) and 3(b), we note that the first minimum in the $I_c(I_{\text{inj}})$ dependence occurs at $I_{\text{inj}}=12.6$ mA for $\theta_1 = \pi/2$ and $I_{\text{inj}}=9.3$ mA for $\theta_1 = \pi$. This difference is in agreement with the expected theoretical ratio:

$$\frac{I_{\text{inj}}(\theta_1 = \pi)}{I_{\text{inj}}(\theta_1 = \pi/2)} = \frac{L^*(\theta_1 = \pi/2)}{L^*(\theta_1 = \pi)} = \frac{3}{4}.$$

As a final remark, we underline the complete analogy between the $I_c(I_{\text{inj}})$ behavior in AJTJs and the $I_c(B_{\text{ext}})$ behavior in a rectangular-shaped Josephson junction, independent from the separation angle θ_1 and, hence, from the distribu-

tion of the magnetic field in the two sectors of the base electrode with annular shape. It is useful to introduce a schematic view of the magnetic field distribution created by the injected current in the AJTJ. This is shown in Fig. 4 for $\theta_1 = \pi$ and for $\theta_1 = \pi/2$, the two cases considered in the experiments. In the case of $\theta_1 = \pi$, there is a radial uniform distribution of the parallel magnetic field in both sectors of the junction. The two fields are equal in magnitude and opposite in direction [see Fig. 4(a)]. When $\theta_1 = \pi/2$, the two fluxes are still equal in magnitude, opposite in direction, but the respective magnetic field intensities are different: the magnetic field intensity is smaller in the larger sector [sector 2 in Fig. 4(b)]. In this situation, the spatial distribution of B_{inj} over the total junction area can be considered as truly nonuniform. Nevertheless, in the general case $\theta_1 \neq \pi$, the intensities of the fields in the two sectors are different, but the two *magnetic fluxes* have the same value $\phi_1 = \phi_2 = L^* I_{\text{inj}}$.

2. $I_c(B_{\text{ext}})$ dependence with injection current at $\theta_1 = \pi$

Now we discuss the dependence of I_c on the external field B_{ext}, when fixed I_{inj} values are maintained at a constant value. This case is relevant to show the similarity with a truly trapped flux behavior of an AJTJ. The measurements were performed at the separation angle of $\theta_1 = \pi$. Figure 5 shows the experimental $I_c(B_{\text{ext}})$ curves by open circles. The experimental dependences of Figs. 5(a)–5(c) were all taken by aligning the direction of B_{ext} to the same direction of the injector leads, i.e., $\theta_f = \pi$. In Fig. 5(a), the injection current satisfies the condition $\phi = \Phi_0$; while in Fig. 5(b), $\phi = 2\Phi_0$. The solid lines of Figs. 5(a) and 5(b) are obtained from Eq. (8) of Ref. 11:
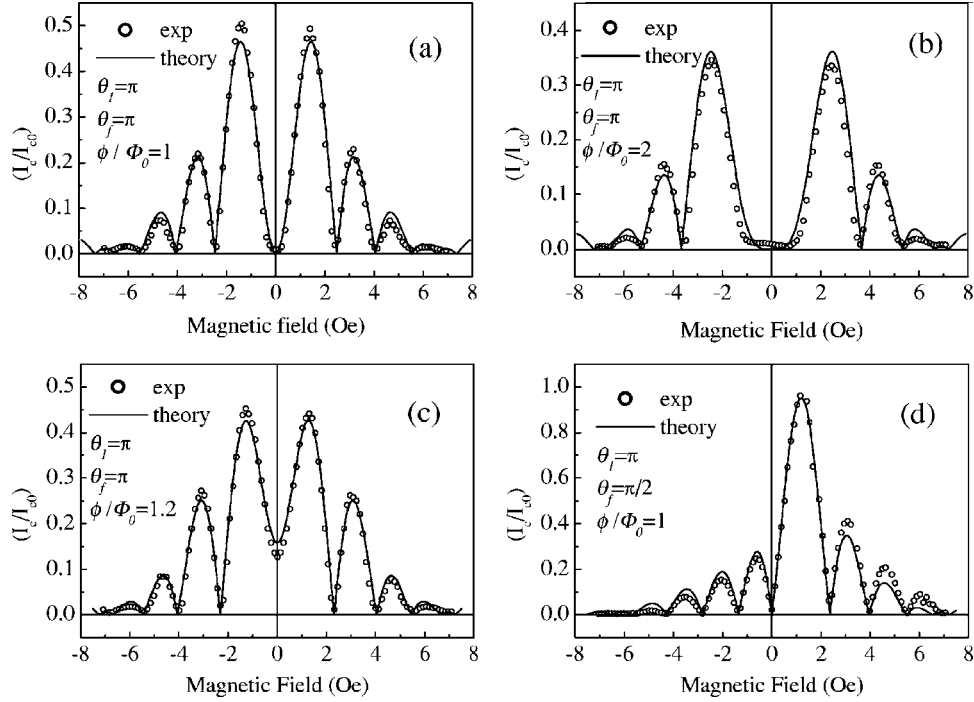
FIG. 5. Josephson critical current versus external magnetic field, $I_c(B_{ext})$ dependences, in the presence of the injection current I_{inj}. Experimental data are plotted by open circles, theoretical curves are shown by solid lines. (a), (b), and (c) represent the results when the injection current was applied through the terminals A and B_2 ($\theta_1 = \pi$) and the external magnetic field was oriented along the injection current leads ($\theta_f = \pi$): (a) $\phi = \Phi_0$; (b) $\phi = 2\Phi_0$; and (c) $\phi = 1.2\Phi_0$. (d): $I_c(B_{ext})$ corresponds to the case in which the injection current, satisfying $\phi = \Phi_0$, was applied through the terminals A and B_2 ($\theta_1 = \pi$) but the magnetic field was oriented perpendicular to the injection leads ($\theta_f = \pi/2$). Theoretical curves in (a) and (b) were calculated by Eq. (28); the solid lines of (c) and (d) are obtained from Eq. (13).

$$\frac{I_c}{I_{c0}} = \left| \frac{2}{(1-\delta^2)} \int_{\delta}^{1} x\,dx\,J_{2n}(xh) \right|, \qquad (28)$$

where $h = B_{ext}/B_0$, $B_0 = \Phi_0/2\pi R_2 d_{eff}$, $x = r/R_2$, and $\delta = R_1/R_2$. Equation (28) is exactly the same result of Eq. (29) of Ref. 16, obtained when $2n$ flux quanta are trapped in one of the two ring electrodes of an annular junction. Thus, the $I_c(B_{ext})$ dependence is the same even if the field configuration is much different in the two cases. In the case of injected current, the magnetic flux changes sign twice, resulting in opposite signs in the two ring sectors; whereas the sign of the flux in the case of trapped flux quanta does not change around the ring. Therefore, the curves correspond to the cases when two [Fig. 5(a)] or four [Fig. 5(b)] magnetic flux quanta were truly trapped into the annular junction. The good agreement observed between theory and experiment confirms that the effect on the Josephson critical current of the injection current corresponding to $\phi = n\Phi_0$ and $\theta_1 = \pi$ reproduces the influence of $2n$ magnetic flux quanta trapped inside the hole of one annular electrode, by reproducing the corresponding current density distribution.

We also measured the $I_c(B_{ext})$ dependence by injecting a current I_{inj} to give $\phi = 1.2\Phi_0$ such that $\phi \neq n\Phi_0$. The obtained experimental dependence is shown in Fig. 5(c) by open circles, and was different from the previous cases. The theoretical curve [solid line of Fig. 5(c)] was calculated directly by general formula Eq. (13) at $I_{inj} = 1.2\Phi_0$.

All $I_c(B_{ext})$ dependences measured at $\theta_f = \pi$ were symmetric with respect to the I_c axis. The asymmetrical $I_c(B_{ext})$ de-

pendence was observed when the external magnetic field was applied perpendicular to the injection leads, i.e., $\theta_f = \pi/2$ [Fig. 5(d), open circles]. In Fig. 5(d), $\phi = \Phi_0$ so that the critical current is zero at zero-external magnetic field. The solid line of Fig. 5(d) represents the result of calculation made by the general Eq. (13) at $\theta_f = \pi/2$ and $\phi = \Phi_0$. Small deviation between experiments and theory, more pronounced for secondary lobes, can be explained by taking into account the experimental error in the definition of the angle θ_f.

In conclusion of the present subsection, an interesting aspect of the injection current case is the possibility to create a field configuration when I_{inj} corresponds to $\phi = n\Phi_0$, as Figs. 5(a) and 5(b) show. In this case, the insertion of fluxon occurs. The field distribution is radial as well as in the truly trapped configuration. However, in the injection current case, the total flux threading the barrier is zero; while in the truly trapped configuration, a net flux exists. The equivalent number of inserted fluxons is always an integer and even in the injection configuration, while any integer number (even and odd) is allowed in the truly trapped configuration.

B. Fiske resonance measurements

Three Fiske resonances at voltage positions $V_1 = 97$ μV, $V_2 = 193$ μV, and $V_3 = 290$ μV were observed in the current-voltage characteristic. During these measurements, the Fiske steps amplitudes were maximized with the magnetic field. We measured the dependence of their maximum amplitude as a function of the injection current I_{inj} for the two separation angles $\theta_1 = \pi/2$ and $\theta_1 = \pi$.
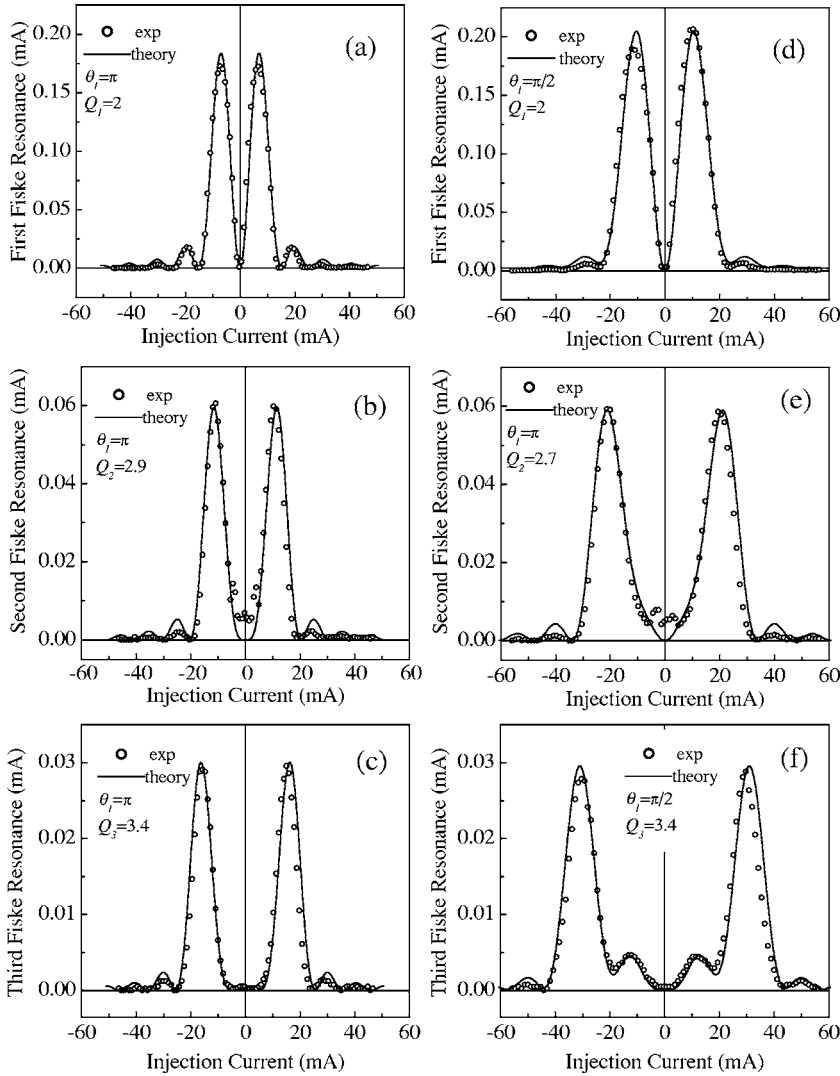
FIG. 6. Experimental dependences of the first, second, and third Fiske resonances on the injection current (open circles). (a), (b), and (c) show the curves measured when the injection current was applied between terminals A and B_2 ($\theta_1 = \pi$) The solid lines are the theoretical curves calculated by Eq. (26). (d), (e), and (f) show the curves measured when the injection current was applied between terminals A and B_1 ($\theta_1 = \pi/2$). The theoretical dependences of (d), (e), and (f) were calculated by the complicated Eq. (25). The quality factors Q_k were used as the fit parameter.

Figures 6(a)–6(c) show the experimental dependence of the amplitudes of the three Fiske resonances on the injection current for $\theta_1 = \pi$ (open circles). By using the best-fit value of d_{eff} and L^* obtained previously from the $I_c(B_{\text{ext}})$ and $I_c(I_{\text{inj}})$ dependences, we calculate the theoretical curves by Eq. (26) [solid line of Figs. 6(a)–6(c)]. We remark that this equation is very similar to the Fiske resonance dependence of a rectangular junction in parallel magnetic field. In using Eq. (26), only the quality factor, Q_k, was a fit parameter. The Q_k values are given in the inset of the figures. We observe that the quality factor slightly increases with the resonance order k. This behavior of Q_k is a consequence of the variation of the junction resistance R_d^k as can be seen from the current-voltage characteristics at the three different voltage values.

Figures 6(d)–6(f) show the experimental dependences of the first, second, and third resonances on the injection current for the separation angle $\theta_1 = \pi/2$. The general expression Eq. (25) is used to plot the theoretical results. Now, the analogy with the formula for rectangular-shaped junctions is lost. One can see the excellent agreement between the experimental results and the theoretical dependences in both cases. We stress that the same Q_1 (first Fiske resonance) and Q_3 (third Fiske resonance) fitting parameters were used for both separa-

ration angles $\theta_1 = \pi/2$ and $\theta_1 = \pi$; whereas only the value of Q_2 for the second Fiske resonance was slightly different between the two separation angles [Fig. 6(e)].

The behavior of the Fiske resonances, expressing the phase dynamics of the junction, is more complex than the static case. The analogy with rectangular junctions is found only when the separation angle is $\theta_1 = \pi$. As we demonstrated theoretically and confirmed experimentally, at $\theta_1 \neq \pi$ the dependence of the Fiske resonances on the injection current is described by the more complicated result of Eq. (25). We note explicitly that the conditions for this case correspond to the excitation of resonances by means of a nonuniform magnetic field.

We found three Fiske resonances in the presence of injected current in the current-voltage curve, which can be interpreted as the three first modes due to the identical difference in the voltage position of the neighbor steps. Such resonances can be interpreted as a result of the interaction between the Josephson current and the electromagnetic standing wave located along the annular junction circumference (no radial modes) (dashed line of Fig. 4).[16] The experimental conditions suggest that the theoretical assumptions of neglecting the dependence on the radial coordinate and of treating the problem in 1D approximation are correct. We

obtained $\bar{c}=0.039c$ for the Swihart velocity from Eq. (24) using the experimental value of the voltage position of the first Fiske resonance. This value is in agreement with the data published in literature for Nb/Al junctions.[17]

We want to return again to the qualitative pictures of the magnetic field distributions presented in Fig. 4. A uniform (equal density) magnetic field distribution at $\theta_1 = \pi$ results in the Fiske resonance behavior similar to the rectangular junction in a parallel magnetic field [Fig. 4(a)]. A nonuniform (different intensity) magnetic field created by the injection current at $\theta_1 \neq \pi$ [the case $\theta_1 = \pi/2$ of Fig. 4(b)] strongly influences the mechanism of the appearance of Fiske resonances so that, in contrast to the Josephson critical current case, the injection current dependence of the Fiske resonances deviates from the expression representing Fiske resonances of a rectangular junction in a uniform magnetic field.

V. CONCLUSIONS

We have theoretically and experimentally studied the dc and ac Josephson effects of an annular tunnel junction with injection current. The results we found in our previous work[11] have been generalized providing the complete analytical expression for the Josephson critical current of an annular junction in the presence of both the injection current and external magnetic field. We have extended the work to investigate the dynamic case, and derived a general analytical expression for Fiske resonances of an annular junction when an injection current is applied. We have fabricated a Nb-based annular Josephson tunnel junction with the possibility to apply the injection current with two separation angles of $\theta_1 = \pi/2$ and of $\theta_1 = \pi$. We have made measurements of the injection current dependences of the Josephson critical current and the Fiske resonances for separation angles $\theta_1 = \pi$ and $\theta_1 = \pi/2$. The experimental data were compared with the theoretical curves calculated by our expressions. We have experimentally confirmed that in case of a *small* annular junction, the injection current modulates the Josephson critical current according to the Fraunhofer pattern at any separation angle between the injection leads. We have demonstrated that only in the case of a separation angle $\theta_1 = \pi$, the injection current dependence of the Fiske resonances is described by the same expression as for

Fiske resonances of a rectangular junction in a parallel uniform magnetic field. Our experiments have fully confirmed the theoretical prediction of the behavior of Fiske resonances in the presence of the injection current both at $\theta_1 = \pi$ and $\theta_1 \neq \pi$.

The method of injection current also allows one to obtain a field configuration corresponding to the one when fluxon trapping occurs. The effect of the injection current on the Josephson critical current at $\phi = n\Phi_0$ and $\theta_1 = \pi$ is similar to the effect of the $2n$ magnetic flux quanta trapped inside the hole of one annular electrode. This can be used in applications, as long as reliable methods of fluxon trapping are not available. The field and current configurations realized have the advantage of being reversible. In the limit in which θ_1 goes to zero, the magnetic field intensity diverges; whereas the surface $d_{\mathrm{eff}}\theta_1 r$ shrinks, in such a way that the flux is kept constant. In this case, the trapping of fluxons can be irreversible, thereby without the need to sustain such a configuration with a continuous injection of circulating current. The investigation presented in this work is a contribution in this direction as well as to a more general understanding of the phenomenology of annular junctions.

Concerning applications, annular junctions with injection current are promising for their use as STJ radiation detectors. The importance of suppressing the Josephson effects in operating STJ detectors, as well as a first attempt to use the annular geometry for STJ detectors, is described in Refs. 6 and 7. The application of the injection current in the case of an annular geometry permits one to suppress both the Josephson critical current and the Fiske resonances and, hence, avoid the necessity of using a magnetic coil for creating the magnetic field. Our investigation indicates that annular junctions with a separation angle of $\theta_1 = \pi$ have the optimal configuration for the suppression of the Josephson effects by a magnetic field with the least possible value.

[1] N. Grønbech-Jensen, P. S. Lomdahl, and M. R. Samuelsen, Phys. Rev. B **43**, 12799 (1991).

[2] N. Grønbech-Jensen, P. S. Lomdahl, and M. R. Samuelsen, Phys. Lett. A **154**, 14 (1991).

[3] Niels Grønbech-Jensen, Phys. Rev. B **45**, 7315 (1992).

[4] E. Kavoussanaki, R. Monaco, and R. J. Rivers, Phys. Rev. Lett. **85**, 3452 (2000).

[5] A. Wallraff, A. Lukashenko, J. Lisenfeld, A. Kemp, Y. Koval, M. V. Fistul, and A. V. Ustinov, Nature (London) **425**, 155 (2003).

[6] C. Nappi and R. Cristiano, Appl. Phys. Lett. **70**, 1320 (1997); L. Frunzio, L. Li, D. E. Prober, I. V. Vernik, M. P. Lisitskii, C. Nappi, R. Cristiano, *ibid.* **79**, 2103 (2001).

[7] M. P. Lisitskiy, C. Nappi, M. Ejrnaes, R. Cristiano, M. Huber, K. Rottler, J. Jochum, F. von Feilitzsch, and A. Barone, Appl. Phys. Lett. **84**, 5464 (2004).

[8] C. Nappi, R. Cristiano, M. P. Lissitski, R. Monaco, and A. Barone, Physica C **367**, 241 (2002).

[9] R. Cristiano, E. Esposito, L. Frunzio, M. Lisitskii, C. Nappi, G. Ammendola, A. Barone, L. Parlato, D. Balashov, and V. N. Gubankov, Appl. Phys. Lett. **74**, 3389 (1999).

[10] A. V. Ustinov, *Controlled and Reversible Insertion of Fluxons into Annular Josephson Junctions, Abstracts of the Satellite Conference to EUCAS, 2001, Physics and Applications of Superconducting Quantum Interference* (Stenungsbaden, Sweden,

2001), p. 32; A. V. Ustinov, Appl. Phys. Lett. **80**, 3153 (2002).

[11] C. Nappi, M. P. Lissitski, and R. Cristiano, Phys. Rev. B **65**, 132516 (2002).

[12] A. Barone and G. Paternò, *Physics and Applications of the Josephson Effects* (Wiley, New York, 1982).

[13] B. A. Malomed and A. V. Ustinov, Phys. Rev. B **69**, 064502 (2004).

[14] I. O. Kulik, JETP Lett. **2**, 84 (1965).

[15] T. Van Duzer and C. W. Turner, *Principles of Superconductive Devices and Circuits*, 2nd Ed. (Prentice-Hall, Englewood Cliffs, New Jersey, 1999).

[16] C. Nappi, R. Cristiano, and M. P. Lisitskii, Phys. Rev. B **58**, 11685 (1998).

[17] J. G. Gijsbertsen, E. P. Houwman, B. B. G. Klopman, J. Flokstra, H. Rogalla, D. Quenter, and S. Lemke, Physica C **249**, 12 (1995).